Journal Name

COMMUNICATION

Spatial Differentiation of Brønsted Acid Sites by Probe Molecule in Zeolite USY using Synchrotron X-ray Powder Diffraction

Received 00th January 20xx,
Accepted 00th January 20xx

DOI: 10.1039/x0xx00000x

www.rsc.org/

Lin Ye, Ivo Teixeira, Benedict T.W. Lo, Pu Zhao, and S.C. Edman Tsang*

By combining synchrotron X-ray powder diffraction, Rietveld refinement and the use of a probe molecule, Brønsted Acid Sites (BAS) of different strengths in steam-treated USY zeolite can be for the first time spatially differentiated: this enables the analysis of different acid-catalysed reactions of dimethylfuran (biomass) by the zeolite using a definitive site blockage strategy.

Acid-base reactions form the primary basis of zeolite catalysis.[1] A wide range of porous zeolitic structures with and without modification have been widely used as microporous catalysts in industry for fuels processing and chemicals manufacture.[2,3] Typically, the acidity and basicity of structurally more robust zeolite Y have been extensively characterized.[3,4] The crystal structure of zeolite Y is generated by connecting sodalite units (sodalite cage with a 2.6 Å window) via hexagonal prisms which forms the empty cavities (supercage with a 7.6 Å window). In general, the catalytically active sites of zeolite Y are the Brønsted acid sites (BAS), which are created through the substitution of silicon (tetravalent) by aluminum (trivalent) in the zeolite Y framework with an acidic proton associated with the bridging oxygen atom of Al-O-Si for charge compensation.[5] A mild steaming treatment is used to improve the hydrothermal stability of the proton formed zeolite Y as the ultra-stable zeolite HY (USY).[6-8] During the steaming treatment, part of framework Al^{3+} was found leaching into the extra-framework positions.[9] Corma et al. attributed the extra-framework Al^{3+} species to the rise of some stronger BAS.[10] Mirodatos et al suggested the superacid sites in dealuminated zeolites resulted from the interactions between protonic sites and extra-framework oxoaluminium deposited in the zeolite pores.[11] On the other hand, using combined *in-situ* X-ray techniques, Bokhoven et al. concluded some extra-framework Al^{3+} species took residence inside the sodalite cage, which could affect the BAS.[12] By combining detailed solid-state NMR studies and theoretical calculations, Deng et al. considered a range of possible oxoaluminium ions and neutral extra-framework species influencing the BAS: some prefer to stay in the supercage, but some occupy the sodalite cages.[13] However, the direct correlation between a particular extra-framework Al^{3+} species and the enhanced BAS cannot be unambiguously assigned due to the limitations of the spatial resolution of the technique. In contrast, there are also some reports claiming that the extra-framework Al^{3+} species only act as spectators, which would not alter the strength of BAS.[14,15] The contradictory views arise mainly fromthe lack of advance characterization tools to link BAS acidity measurement with structure in 3-D local and global atomic arrangements. Practically, acidity measurement is commonly done with temperature programmed desorption (TPD) of basic probe molecules such as ammonia, pyridine or TMP. However, the deconvolution of generally complex desorption peaks to differentiate strength and quantity of BAS sites is frequently challenging. More importantly, although some spectroscopic techniques can be used to identify the nature of acidic sites, they cannot generate the spatial information of the acidic sites without controversy.[10, 11, 13] This posts huge difficulties to carry out rational analysis of BAS to correlate important specific catalytic reactions taken place in zeolites with confidence, let alone the exciting site engineering. For example, biomass derived furans can be catalyzed by BAS into valuable aromatic products by a Diels-Alder cycloaddition with ethylene over zeolite.[16] However, some BAS in the zeolite can also accelerate the side reactions of 2,5-dimethylfuran (DMF) hydrolysis into ketones (Fig. S4). No rational differentiation of these BAS in zeolites is yet achieved.

Recently, we and others have shown that high-resolution synchrotron X-ray powder diffraction (SXRD) allows the elucidation of organic/inorganic adsorbate structure in zeolites and MOFs.[17-19] Combined with Rietveld refinement, the atomic spatial information and the local bonding interaction between organic adsorbate and zeolite acid site can be visualized at the

Department of Chemistry, University of Oxford, Oxford, OX1 3QR, UK
**E-mail: edman.tsang@chem.ox.ac.uk*

Electronic Supplementary Information (ESI) available: Solid-state NMR, synchrotron XRD and Rietveld refinement of USY before and after pyridine adsorption, Synchrotron XRD and Rietveld refinement of USY after potassium loading, references. See DOI: 10.1039/x0xx00000x

This journal is © The Royal Society of Chemistry 20xx

Please do not adjust margins

same time, which could not be provided by most spectroscopies (IR, Raman, NMR) and thermal methods (TPD, TGA). In this work, the spatial distribution and the acidic strength of BAS in dealuminated USY500 and USY15, of different Si/Al ratios are investigated by using SXRD in combination with the basic pyridine probe molecule. For *the first time*, a four coordinated (CN) extra-framework Al^{3+} is identified in the sodalite cage of USY15. It directly polarizes the surrounding BAS oxygen atoms in the first coordination sphere pointing towards the supercage. This leads to enhanced BAS strength (longer distance with the adsorbed pyridinium ion in the pore). On the other hand, USY500 shows only weak BAS, giving corresponding shorter distance with pyridine of more covalent character. By adopting a strategy of partially/totally blockage of the BAS of different acid strengths with K^+, the products distribution can clearly reflect that Diels-Alder cycloaddition is catalysed by the strong acid sites while the hydrolysis of furan takes place over the weak acid sites.

USY500 (Si/Al = 325) and USY15 (Si/Al = 7.3) were obtained from TOSOH. ^{27}Al MAS NMR can provide the local information about the Al distribution and coordination in zeolites.[12,20,21] Figures 1a, 1b show the ^{27}Al MAS NMR spectra of USY500 and USY15. There is only one peak appearing at 62.8 ppm in the spectrum of USY500 (Fig. 1a). It belongs to the 4-CN framework Al^{3+} species (framework BAS).[21] Due to the low Al concentration of USY500, the signal-to-noise ratio of the ^{27}Al NMR spectrum is poor (Fig. 1a). On the other hand, two well-defined peaks at 62.3 ppm and 1.2 ppm corresponding to 4-CN framework Al^{3+} species (framework BAS) and 6-CN extra-framework Al^{3+} respectively can be clearly seen in the spectrum of USY15 (Fig. 1b). An additional peak at 32.3 ppm can also be detected corresponding to the distorted 4 or 5-CN Al^{3+} species.[21] Peak deconvolution in Fig. 1b shows that around 39% of Al^{3+} are 4-CN framework species, 13% are distorted 4,5-CN species and 48% are the 6-CN extra-framework Al^{3+} species in USY15. According to ICP analysis, there are 23 Al atoms in each USY15 unit cell, therefore it corresponds to 9 4-CN framework Al^{3+}, 3 distorted 4,5-CN Al^{3+} and 11 6-CN extra-framework Al^{3+} per unit cell. In contrast, there is only 0.6 4-CN framework Al^{3+} per unit cell in USY500.

It is thus evident that there are at least two types of extra-framework Al^{3+} species in USY15 along with the observed framework BAS, whereas there is only the framework BAS detected in USY500 by ^{27}Al NMR analysis. ^{31}P NMR with trimethylphosphine oxide (TMPO) was also applied to characterize the acidic nature of USY500 and USY15.[22] Because of the low Al^{3+} concentration in USY500, ^{31}P NMR spectrum (Fig. 1c) mainly shows a peak due to the TMPO physisorption (41.7 ppm). However, the deconvolution of the spectrum of TMPO adsorbed USY15 (Fig. 1d) clearly indicates resolved peaks are from TMPO-Lewis acid 6-CN extra-framework adduct (39.3 ppm), TMPO physisorption (41.9 ppm) and two TMPO-BAS adducts at 54.1 ppm and 65.3 ppm, respectively. In other words, USY15 again shows two types of BAS, a relatively weak framework BAS (54.1 ppm, relates to the 4-CN framework Al^{3+}) and a strong BAS (65.3 ppm, relates to the 4-CN extra-framework Al^{3+}) with the ratio 2.4: 1 (versus ca. 3.0: 1 derived

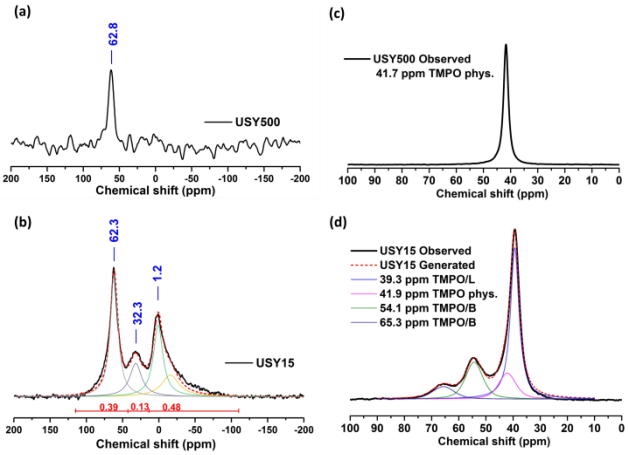


Fig. 1. ^{27}Al MAS NMR spectra of (a) USY500 and (b) USY15, ^{31}P MAS NMR spectra and the deconvolution curves of (trimethylphosphine oxide) TMPO adsorbed on (c) USY500 and (d) USY15.

from ^{27}Al NMR). USY15 also has the characteristic Lewis acid sites (39 ppm) of the 6-CN extra-framework Al^{3+} species.

This observation matches with the previous characterization[13,23] that two BAS with the signals at 5.0 and 4.3 ppm in ^{1}H NMR were noted from the steam-treated HY zeolite. HY has a highly symmetric structure with one spatial statistical T site. When Al substitutes Si, the BAS should generate only one type of acidic strength. However, USY15 (HY15 after steam treatment) at the high Al/Si ratio clearly displays two types of BAS acidic strengths, which hints the dealuminated Al^{3+} in proximity somehow enhances the acidic strength of BAS, confirming the previous findings from Bokhoven, Deng, and other researchers.[10,12,13,24] However, as discussed, no direct correlation between this encapsulated Al^{3+} in the sodalite cage and the exposed BAS site and adsorbate in the supercage can be undisputedly elucidated due to the spatial limitations of the spectroscopic techniques.

As a result, synchrotron X-ray powder diffraction (SXRD) was employed in this work. The SXRD patterns of USY500 (Fig. S3a) and USY15 (Fig. S3b) were fitted by the Rietveld method using TOPAS software (Bruker AXS, version 5), see details in the supplementary information section 3. Both refinements started from the zeolite Y (purely siliceous) crystal structure.[25] The acceptable R-factors, R_{wp} 8.916% and 9.561% and low thermal factors clearly show the high quality and accuracy of the refinement. In Fig. S3c, no extra-framework Al^{3+} species exists in USY500, which is consistent with the ^{27}Al NMR result. On the contrary, extra-framework Al^{3+} can be found in the sodalite cages of USY15 with 2.17(11) Al^{3+} per unit cell. Rietveld refinement has also been applied to locate the adsorbed pyridine molecules with respect to the positions of the BAS. Their inter-atomic distances may reflect the nature and strength of the acid site adducts.[17] The SXRD refined patterns of pyridine-adsorbed USY500 (Fig. 2a) and USY15 (Fig. 2b) in typical zoom region of 20 – 55° 2θ illustrate the high quality of the refinements within acceptable errors (see supplementary information section 3). The refined structure of USY500 shows

This journal is © The Royal Society of Chemistry 20xx

Please do not adjust margins

Please do not adjust margins

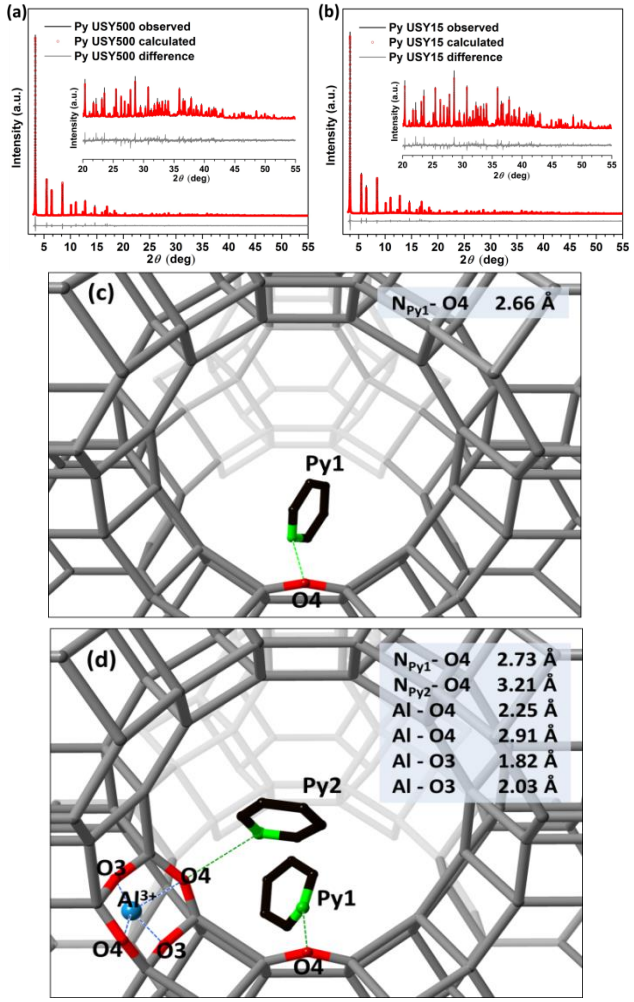


Fig. 2. SXRD diffraction patterns and Rietveld refinement data of (a) USY500 and (b) USY15 after pyridine adsorption. The 20 – 55° 2θ region is zoomed into illustrate the quality of the refinement. The structures of (c) USY500 and (d) USY15 with stick models without symmetrically appearing 4-CN extra-framework Al3+ species and pyridine. Grey represents the USY; Blue ball represents Al (4-CN extra-framework Al^{3+} species); Green represents N of pyridine, Black represents C of pyridine.

only one pyridine site (Py1) located in supercage, interacting with the framework O4 (BAS) with the shortest distance of 2.66(1) Å N_{Py}-$O_{framework}$ (Fig. 2c). It is noted that this O4 atom is a part of the vertex of a sodalite cage exposed to the supercage whereas no encapsulated pyridine is found inside the sodalite, presumably due to its large dynamic size (4.9 Å). Due to the low electron density of H atoms, it is impossible to locate them directly. However, the lone pair electrons of nitrogen in pyridine probe molecule in the supercage can act as a Brønsted base to bind with the proton of the BAS (Al-O(H)-Si) of the sodalite cage to form a PyH^+ species. This interaction with Al-O^--Si can be either electrostatic or covalent depending on the strength of the BAS. Additionally, there are 0.59(1) pyridine per unit cell in USY500. This is calculated from the site occupancy and symmetry multiplicity of Py1 obtained by the refinement. This corresponds excellently to 0.6 framework Al^{3+} per unit cell evaluated by the ^{27}Al MAS NMR.

Interestingly, the refined structure of pyridine-adsorbed USY15 shows an additional distorted 4-CN extra-framework Al^{3+} site in a sodalite cage that is normally unoccupied. In addition, there are also two distinctive pyridine sites in the supercage (Fig. 2d), see detailed refinement procedure in supporting information section S3. In fact, Al^{3+} and $Al(OH)^{2+}$ have been used for the refinement, as these two species could theoretically pass through the window of the sodalite cage. It is found that Al^{3+} gives better SXRD fitted than $Al(OH)^{2+}$. Al^{3+} gives a significant lower R_{wp} value. This encapsulated Al^{3+} appears to bind with the two O3 and O4 in the first coordination sphere of the sodalite cage, as shown Fig. 2d. Two pyridine sites are found closest to the framework O4 atoms (sodalite cages with and without encapsulated Al^{3+}) in the 12-membered ring. The measured distances of N_{Py1}-O4 and N_{Py2}-O4 are 2.73(1) Å and 3.21(2) Å, respectively. The Py1 site position and N_{Py1}-O4 distance (2.73(1) Å) in USY15 without Al^{3+}- sodalite are the same as the Py1 site in USY500, which means this weaker Brønsted acid site is the typical BAS from the Al substituted the framework Si site.

Notice that the new Py2 site with a longer N_{Py2}-O4 distance (3.21(2) Å) of stronger Brønsted acidity is clearly structurally linked to the extra-framework Al^{3+} through the first coordinated BAS O4 at the interface between Al^{3+}-sodalite and supercage. It is conceivable from the corresponding observed atomic arrangement that the additional Lewis acidity of the extra-framework Al^{3+} inside the sodalite cage is expected to polarize its nearby BAS O4 at the vertex, leading to the higher propensity for proton to be released to pyridine from this strong BAS. Accordingly, the decrease in covalency between O4(H) with the increase in electrostatic interaction render the $O4^-\cdots Py2H^+$ longer than N_{Py1}-O4. Although we cannot rule out the existence of other disordered oxoaluminium ions or neutral species deposited in close proximity to O4, influencing this BAS position, the comparable amount of Py2 (2.13(4) per unit cell) and the extra-framework Al^{3+} in sodalite cage (2.17(11) per unit cell) evaluated by the refinement reveals the direct structural link to the enhanced BAS acidity.

The use of Lewis acid species to increase Brønsted acidity is well-demonstrated in a number of homogeneous super-acid systems such like $AlCl_3$-HCl and SbF_5-HF[26, 27] , but is still debatable over solid zeolite systems. We believe this direct observation of the acid-base adduct between pyridine probe and BAS O4 modified by the encapsulated Lewis acid Al^{3+} in sodalite cage can be evident to support such preposition in the literature that has not been obtained by other techniques. As it is evident that USY15 gives an additional stronger BAS when compare with USY500, strategic sites blockage in selective manner may allow the rational tailoring of specific BAS for zeolitic catalysis. Typical BAS dependent reactions such as the catalytic conversion of 2,5-dimethylfuran (DMF) into aromatics by Diels-Alder cycloaddition with ethylene, *in-situ* generated by dehydration of ethanol was therefore studied.[16] This desirable reaction involves the DMF cycloaddition, followed by the oxa-norbornene dehydration into xylene over BAS sites in the USY. Previous work has shown the bicyclo norbornene dehydration is the rate limiting step at low BAS concentration.

This journal is © The Royal Society of Chemistry 20xx

Please do not adjust margins

Please do not adjust margins

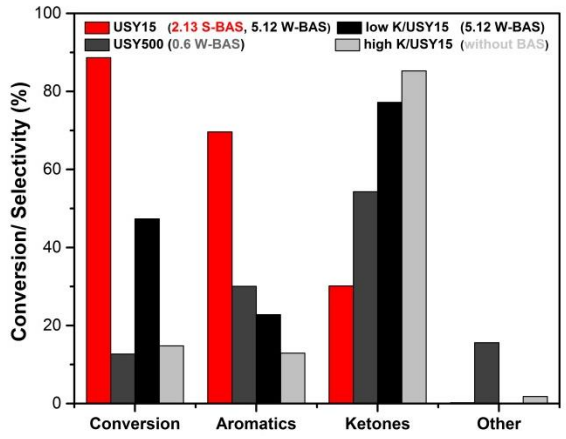


Fig. 3. Conversion and selectivity for DMF transformation into aromatics catalyzed by USY15, USY500, low K/USY15 and high K/USY15. Reaction conditions: 250 °C, molar ratio ethanol/DMF 1:1 and reaction time 24 h. Number in bracket represents BAS/unit cell. S: strong BAS; W: weak BAS.

However, some BAS can also catalyze the hydrolysis of DMF into 2,5-hexanedione (Fig. S4), which can be further converted to a

range of ketones as side products.[27] It is interesting to find that our zeolites show quite different kinetics for the DMF conversion (Fig. S5): the USY15 shows a reaction rate of 0.073 mol.g^{-1}_{cat}.h^{-1}, while the USY500 shows a much slower rate (0.012 mol.g^{-1}_{cat}.h^{-1}). This difference is anticipated, since the zeolite USY15 (2.13 strong BAS and 5.11 weak BAS per unit cell, giving a total BAS concentration of 0.63 mmol g^{-1}) has a higher concentration of BAS than the USY500 (0.6 weak BAS per unit cell giving a BAS concentration of 0.052 mmol g^{-1}, see Table S6). This agrees with the previous observation of the BAS concentration dependent rate for this reaction.[28]

However, the product distributions are also drastically different: zeolite USY15 shows a clear trend to promote aromatic products, while USY500 favours ketones formation (Fig. 3), mainly the formation of the 2,5-hexanedione (41.2%). The presence of strong BAS in USY15 associated with encapsulated extra-framework Al^{3+} in sodalite cages may facilitate the protonation for the higher energetic C-O bond cleavages in the ether activation to dehydrate the oxa-norbornene into xylene, accounting for higher aromatic selectivity. In order to ascertain the major role(s) of the strong and weak BAS, a site blockage strategy was implemented. Two USY15 samples were prepared by the partial (blocking the strong BAS of the extra-framework Al^{3+}) and total replacement of the Brønsted acidic protons (blocking all BAS protons) by K^+. The crystallographic evidence (see supporting information section 5.1 and 5.2) confirms the ultra-specificity for strong BAS blockage by K^+ in the partial BAS replaced sample. The partial exchanged USY15 shows a higher conversion (47.3%) and higher reaction rate (0.06 mol.g^{-1}_{cat}.h^{-1}) than that of USY500 as it still contains higher quantity of weak BAS. Interestingly, the product distribution shifts to ketones (77.2%) since the breakage of two strong C-O bonds in the bridge ether intermediate cannot be overcome by the weak BAS which only favours hydrolysis reactions that require lower activation energy. As expected, the sample with the complete exchange of protons with K^+ shows a low activity, favouring the ketones formation.

In summary, synchrotron X-ray powder diffraction combined with probe molecule could act as a new tool to enable a rational but simple site blockage strategy in a quantitative manner to interrogate and optimize complex reactions catalysed by zeolites, leading to superior catalytic performances.

Notes and references

1 A. K. Cheetham, G. Ferey and T. Loiseau, *Angew. Chem. Int. Ed.*, 1999, **38**, 3268-3292.
2 A. Corma, *Chem. Rev.*, 1995, **95**, 559-614.
3 N. Hosseinpour, Y. Mortazavi, A. Bazyari and A. A. Khodadadi, *Fuel Process. Technol.*, 2009, **90**, 171-179.
4 C. Costa, J. M. Lopes, F. Lemos and F. R. Ribeiro, *J. Mol. Catal. A-Chem.*, 1999, **144**, 207-220.
5 J. W. Ward, *J. Catal.* , 1967, **9**, 225-236.
6 R. A. Beyerlein, G. B. McVicker, L. N. Yacullo and J. J. Ziemiak, *J. Phys. Chem.*, 1988, **92**, 1967-1970.
7 S. J. Decanio, J. R. Sohn, P. O. Fritz and J. H. Lunsford, *J. Catal.* , 1986, **101**, 132-141.
8 J. R. Sohn, S. J. Decanio, P. O. Fritz and J. H. Lunsford, *J. Phys. Chem.*, 1986, **90**, 4847-4851.
9 J. Sanz, V. Fornes and A. Corma, *J. Chem. Soc.-Faraday Trans. I*, 1988, **84**, 3113-3119.
10 A. Corma, V. Fornes and F. Rey, *Appl. Catal.* , 1990, **59**, 267-274.
11 C. Mirodatos and D. Barthomeuf, *J. Chem. Soc.-Chem. Commun.*, 1981, DOI: 10.1039/c39810000039, 39-40.
12 G. Agostini, C. Lamberti, L. Palin, M. Milanesio, N. Danilina, B. Xu, M. Janousch and J. A. van Bokhoven, *J. Am. Chem. Soc.*, 2010, **132**, 667-678.
13 S. H. Li, A. M. Zheng, Y. C. Su, H. L. Zhang, L. Chen, J. Yang, C. H. Ye and F. Deng, *J. Am. Chem. Soc.*, 2007, **129**, 11161-11171.
14 M. A. Kuehne, H. H. Kung and J. T. Miller, *J. Catal.* , 1997, **171**, 293-304.
15 M. J. Remy, D. Stanica, G. Poncelet, E. J. P. Feijen, P. J. Grobet, J. A. Martens and P. A. Jacobs, *J. Phys. Chem.*, 1996, **100**, 12440-12447.
16 I. F. Teixeira, B. T. W. Lo, P. Kostetskyy, M. Stamatakis, L. Ye, C. C. Tang, G. Mpourmpakis and S. C. E. Tsang, *Angew. Chem. Int. Ed.*, 2016, **55**, 13061-13066.
17 B. T. W. Lo, L. Ye, J. Qu, J. Sun, J. Zheng, D. Kong, C. A. Murray, C. C. Tang and S. C. E. Tsang, *Angew. Chem. Int. Ed.*, 2016, **55**, 1-5.
18 S. H. Yang, J. Sun, A. J. Ramirez-Cuesta, S. K. Callear, W. I. F. David, D. P. Anderson, R. Newby, A. J. Blake, J. E. Parker, C. C. Tang and M. Schroeder, *Nature Chem.*, 2012, **4**, 887-894.
19 L. Ye, B. T. W. Lo, J. Qu, I. Wilkinson, T. Hughes, C. A. Murray, C. C. Tang and S. C. E. Tsang, *Chem. Commun.*, 2016, **52**, 3422-3425.
20 J. Klinowski, *Chem. Rev.*, 1991, **91**, 1459-1479.
21 S. H. Li, A. M. Zheng, Y. C. Su, H. J. Fang, W. L. Shen, Z. W. Yu, L. Chen and F. Deng, *Phys. Chem. Chem. Phys.*, 2010, **12**, 3895-3903.
22 E. F. Rakiewicz, A. W. Peters, F. Wormsbecher, K. J. Sutovich and K. T. Mueller, *J. Phys. Chem. B*, 1998, **102**, 2890-2896.
23 D. Freude, M. Hunger, H. Pfeifer and W. Schwieger, *Chem. Phys. Lett.*, 1986, **128**, 62-66.
24 D. L. Bhering, A. Ramirez-Solis and C. J. A. Mota, *Journal of Physical Chemistry B*, 2003, **107**, 4342-4347.
25 M. Colligan, P. M. Forster, A. K. Cheetham, Y. Lee, T. Vogt and J. A. Hriljac, *J. Am. Chem. Soc.*, 2004, **126**, 12015-12022.
26 S. Raugei and M. L. Klein, *J. Phys. Chem. B*, 2002, **106**, 11596-11605.
27 A. S. Berenblyum, E. A. Katsman and Y. Z. Karasev, *Appl. Catal. A- Gen.*, 2006, **315**, 128-134.
28 R. E. Patet, N. Nikbin, C. L. Williams, S. K. Green, C.-C. Chang, W. Fan, S. Caratzoulas, P. J. Dauenhauer and D. G. Vlachos, *ACS Catal.*, 2015, **5**, 2367-2375.

This journal is © The Royal Society of Chemistry 20xx

Please do not adjust margins